

# LEARNING ALGEBRAIC REPRESENTATION FOR SYSTEMATIC GENERALIZATION IN ABSTRACT REASONING

**Anonymous authors**

Paper under double-blind review

## ABSTRACT

Is intelligence realized by connectionist or classicist? While connectionist approaches have achieved superhuman performance, there has been growing evidence that such task-specific superiority is particularly fragile in *systematic generalization*. This observation lies in the central debate (Fodor & McLaughlin, 1990; Fodor et al., 1988) between connectionist and classicist, wherein the latter continually advocates an *algebraic* treatment in cognitive architectures. In this work, we follow the classicist’s call and propose a hybrid approach to improve systematic generalization in reasoning. Specifically, we showcase a prototype with algebraic representation for the abstract spatial-temporal reasoning task of Raven’s Progressive Matrices (RPM) and present the ALgebra-Aware Neuro-Semi-Symbolic (ALANS) learner. The ALANS learner is motivated by abstract algebra and the representation theory. It consists of a neural visual perception frontend and an algebraic abstract reasoning backend: the frontend summarizes the visual information from object-based representation, while the backend transforms it into an algebraic structure and induces the hidden operator on the fly. The induced operator is later executed to predict the answer’s representation, and the choice most similar to the prediction is selected as the solution. Extensive experiments show that by incorporating an algebraic treatment, the ALANS learner outperforms various pure connectionist models in domains requiring systematic generalization. We further show that the algebraic representation learned can be decoded by isomorphism and used to *generate* an answer.

## 1 INTRODUCTION

“Thought is in fact a kind of Algebra.”

—William James (James, 1891)

Imagine you are given two alphabetical sequences of “ $c, b, a$ ” and “ $d, c, b$ ”, and asked to fill in the missing element in “ $e, d, ?$ ”. In nearly no time will one realize the answer to be  $c$ . However, more surprising for human learning is that, effortlessly and instantaneously, we can “freely generalize” (Marcus, 2001) the solution to any partial consecutive ordered sequences. While believed to be innate in early development for human infants (Marcus et al., 1999), such systematic generalizability has constantly been missing and proven to be particularly challenging in existing connectionist models (Bahdanau et al., 2019; Lake & Baroni, 2018). In fact, such an ability to entertain a given thought and semantically related contents strongly implies an abstract algebra-like treatment (Fodor et al., 1988); in literature, it is referred to as the “language of thought” (Fodor, 1975), “physical symbol system” (Newell, 1980), and “algebraic mind” (Marcus, 2001). However, in stark contrast, existing connectionist models tend only to capture statistical correlation (Chollet, 2019; Kansky et al., 2017; Lake & Baroni, 2018), rather than providing any account for a structural inductive bias where systematic algebra can be carried out to facilitate generalization.

This contrast instinctively raises a question—what constitutes such an *algebraic* inductive bias? We argue that the foundation of the modeling counterpart to the algebraic treatment in early human development (Marcus, 2001; Marcus et al., 1999) lies in algebraic computations set up on mathematical axioms, a form of formalized human intuition and the starting point of modern mathematical

reasoning (Heath et al., 1956; Maddy, 1988). Of particular importance to the basic building blocks of algebra is the Peano Axiom (Peano, 1889). In the Peano Axiom, the essential components of algebra, the algebraic set and corresponding operators over it, are governed by three statements: (1) the existence of at least one element in the field to study (“zero” element), (2) a successor function that is recursively applied to all elements and can, therefore, span the entire field, and (3) the principle of mathematical induction. Building on such a fundamental axiom, we begin to form the notion of an algebraic set and induce the operator along with it to construct an algebraic structure. We hypothesize that such a treatment of algebraic computations set up on fundamental axioms is essential for a model’s systematic generalizability, the lack of which will only make it sub-optimal.

To demonstrate the benefits of such an algebraic treatment in systematic generalization, we showcase a prototype for Raven’s Progressive Matrices (RPM) (Raven, 1936; Raven & Court, 1998), an exemplar task for abstract spatial-temporal reasoning (Santoro et al., 2018; Zhang et al., 2019a). In this task, an agent is given an incomplete  $3 \times 3$  matrix consisting of eight context panels with the last one missing, and asked to pick one answer from a set of eight choices that best completes the matrix. Human’s reasoning capability of solving this abstract reasoning task has been commonly regarded as an indicator of “general intelligence” (Carpenter et al., 1990) and “fluid intelligence” (Hofstadter, 1995; Jaeggi et al., 2008; Spearman, 1923; 1927). In spite of the task being one that ideally requires abstraction, algebraization, induction, and generalization (Carpenter et al., 1990; Raven, 1936; Raven & Court, 1998), recent endeavors unanimously propose pure connectionist models that attempt to circumvent such intrinsic cognitive requirements (Hu et al., 2020; Santoro et al., 2018; Wang et al., 2020; Wu et al., 2020; Zhang et al., 2019a;b; Zheng et al., 2019). However, these methods’ inefficiency is also evident in systematic generalization; they struggle to extrapolate to domains beyond training, as pointed out in (Santoro et al., 2018; Zhang et al., 2019b) and shown in this paper.

To address the issue, we introduce the ALgebra-Aware Neuro-Semi-Symbolic (ALANS) learner. At a high-level, the ALANS learner is embedded in a general neuro-symbolic architecture (Han et al., 2019; Mao et al., 2019; Yi et al., 2020; 2018) but has on-the-fly operator learnability and hence semi-symbolic. Specifically, it consists of a neural visual perception frontend and an algebraic abstract reasoning backend. For each RPM instance, the neural visual perception frontend first slides a window over each panel to obtain the object-based representation (Kansky et al., 2017; Wu et al., 2017) for every object. A belief inference engine latter aggregates all object-based representation in each panel to produce the probabilistic *belief state*. The algebraic abstract reasoning backend then takes the belief states of the eight context panels, treats them as snapshots on an algebraic structure, lifts them into a matrix-based algebraic representation built on the Peano Axiom and the representation theory (Humphreys, 2012), and induces the hidden operator in the algebraic structure by solving an inner optimization (Bard, 2013; Colson et al., 2007). The algebraic representation for the answer is predicted by executing the induced operator: its corresponding set element is decoded by isomorphism established in the representation theory, and the final answer is selected as the one most similar to the prediction.

The ALANS learner enjoys several benefits in abstract reasoning with an algebraic treatment:

1. Unlike previous monolithic models, the ALANS learner offers a more interpretable account of the entire abstract reasoning process: the neural visual perception frontend extracts object-based representation and produces belief states of panels by explicit probability inference, whereas the algebraic abstract reasoning backend induces the hidden operator in the algebraic structure. The corresponding representation for the final answer is obtained by executing the induced operator, and the choice panel with minimum distance is selected. This process much resembles the top-down bottom-up strategy in human reasoning: humans reason by inducing the hidden relation, executing it to generate a feasible solution in mind, and choosing the most similar answer available (Carpenter et al., 1990). Such a strategy is missing in recent literature (Hu et al., 2020; Santoro et al., 2018; Wang et al., 2020; Wu et al., 2020; Zhang et al., 2019a;b; Zheng et al., 2019).
2. While keeping the semantic interpretability and end-to-end trainability in existing neuro-symbolic frameworks (Han et al., 2019; Mao et al., 2019; Yi et al., 2020; 2018), ALANS is what we call semi-symbolic in the sense that the symbolic operator can be learned and concluded on the fly without manual definition for every one of them. Such an inductive ability also enables a greater extent of the desired generalizability.
3. By decoding the predicted representation in the algebraic structure, we can also generate an answer that satisfies the hidden relation in the context.

This work makes three major contributions: (1) We propose the ALANS learner. Compared to existing monolithic models, the ALANS learner adopts a neuro-semi-symbolic design, where the problem-solving process is decomposed into neural visual perception and algebraic abstract reasoning. (2) To demonstrate the efficacy of incorporating an algebraic treatment in abstract spatial-temporal reasoning, we show the superior systematic generalization ability of the proposed ALANS learner in various extrapolatory RPM domains. (3) We present analyses into both neural visual perception and algebraic abstract reasoning. We also show the generative potential of ALANS.

## 2 RELATED WORK

### 2.1 QUEST FOR SYMBOLIZED MANIPULATION

The idea to treat thinking as a mental language can be dated back to Augustine (Augustine, 1876; Wittgenstein, 1953). Since the 1970s, this school of thought has undergone a dramatic revival as the quest for symbolized manipulation in cognitive modeling, such as “language of thought” (Fodor, 1975), “physical symbol system” (Newell, 1980), and “algebraic mind” (Marcus, 2001). In their study, connectionist’s task-specific superiority and inability to generalize beyond training (Chollet, 2019; Kansky et al., 2017; Santoro et al., 2018; Zhang et al., 2019a) have been hypothetically linked to a lack of such symbolized algebraic manipulation (Chollet, 2019; Lake & Baroni, 2018; Marcus, 2020). With evidence that an algebraic treatment adopted in early human development (Marcus et al., 1999) can potentially address the issue (Bahdanau et al., 2019; Mao et al., 2019; Marcus, 2020), classicist (Fodor et al., 1988) approaches for generalizable reasoning used in programs (McCarthy, 1960) and blocks world (Winograd, 1971) have resurrected. As a hybrid approach to bridge connectionist and classicist, recent developments lead to neuro-symbolic architectures. In particular, the community of theorem proving has been one of the earliest to endorse the technique (Garcez et al., 2012; Rocktäschel & Riedel, 2017; Serafini & Garcez, 2016):  $\partial$ ILP (Evans & Grefenstette, 2018) and NLM (Dong et al., 2019) make inductive programming end-to-end and DeepProbLog (Manhaeve et al., 2018) connects learning and reasoning, the latter of which is closely related to our work, with its differentiable logic inference used in our belief inference engine. Recently, Hudson & Manning (2019) propose NSM for visual question answering where a probabilistic graph is used for reasoning. Yi et al. (2018) demonstrate a neuro-symbolic prototype for the same task where a perception module and a language parsing module are separately trained, with the predefined logic operators associated with language tokens chained to process the visual information. Mao et al. (2019) soften the predefined operators to afford end-to-end training with only question answers. Han et al. (2019) use the hybrid architecture for metaconcept learning. Yi et al. (2020) and Chen et al. (2021) show how neuro-symbolic models can handle explanatory, predictive, and counterfactual questions in temporal and causal reasoning. Lately, NeSS (Chen et al., 2020) exemplifies an algorithmic stack machine that can be used to improve generalization in language learning. ALANS follows the classicist’s call but adopts a neuro-*semi*-symbolic architecture: it is end-to-end trainable as opposed to Yi et al. (2020; 2018) and the operator can be learned and concluded on the fly without manual specification.

### 2.2 ABSTRACT VISUAL REASONING

Recent works by Santoro et al. (2018) and Zhang et al. (2019a) arouse the community’s interest in abstract visual reasoning, where the task of Raven’s Progressive Matrices (RPM) is introduced as such a measure for intelligent agents. Initially proposed as an intelligence quotient test for humans (Raven, 1936; Raven & Court, 1998), RPM is believed to be strongly correlated with human’s general intelligence (Carpenter et al., 1990) and fluid intelligence (Hofstadter, 1995; Jaeggi et al., 2008; Spearman, 1923; 1927). Early RPM-solving systems employ symbolic representation based on hand-designed features and assume access to the underlying logics (Carpenter et al., 1990; Lovett & Forbus, 2017; Lovett et al., 2010; 2009). Another stream of research on RPM recruits similarity-based metrics to select the most similar answer from the choices (Little et al., 2012; McGreggor & Goel, 2014; McGreggor et al., 2014; Mekik et al., 2018; Shegheva & Goel, 2018). However, their hand-defined visual features are unable to handle uncertainty from imperfect perception, and directly assuming access to the logic operations simplifies the problem. Recently proposed data-driven approaches arise from the availability of large datasets: Santoro et al. (2018) extend a pedagogical RPM generation method (Wang & Su, 2015), whereas Zhang et al. (2019a) use a stochastic image

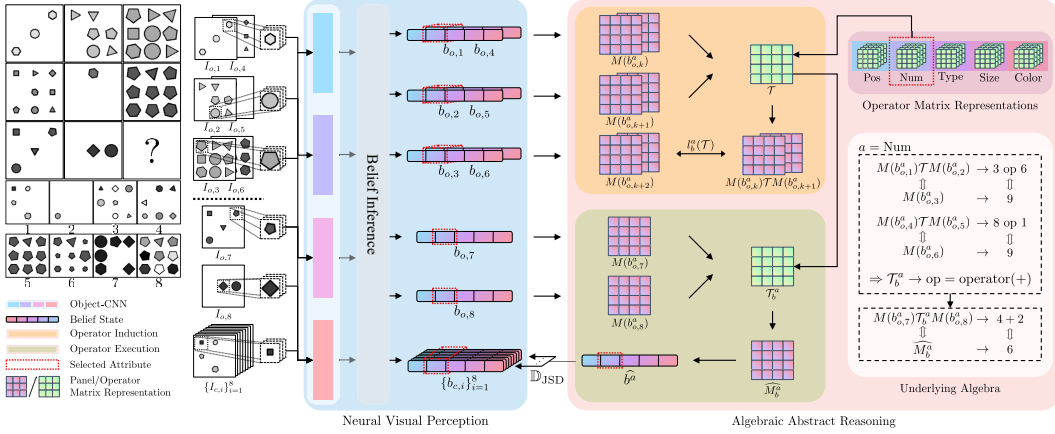


Figure 1: An overview of the ALANS learner. For an RPM instance, the neural visual perception module produces the belief states for all panels: an object CNN extracts object attribute distributions for each image region, and a belief inference engine marginalizes them out to obtain panel attribute distributions. For each panel attribute, the algebraic abstract reasoning module transforms the belief states into matrix-based algebraic representation and induces hidden operators by solving inner optimizations. The answer representation is obtained by executing the induced operators, and the choice most similar to the prediction is selected as the solution. An example of the underlying discrete algebra and its correspondence is also shown on the right.

grammar (Zhu et al., 2007) and introduce structural annotations in it, which Hu et al. (2020) further refine to avoid shortcut solutions by statistics in candidate panels. Despite the fact that RPM intrinsically requires one to perform abstraction, algebraization, induction, and generalization, existing methods bypass such cognitive requirements using a single feedforward pass in connectionist models: Santoro et al. (2018) use a relational module (Santoro et al., 2017), Steenbrugge et al. (2018) augment it with a VAE (Kingma & Welling, 2013), Zhang et al. (2019a) assemble a dynamic tree, Hill et al. (2019) arrange the data in a contrastive manner, Zhang et al. (2019b) propose a contrast module, Zheng et al. (2019) formulate it in a student-teacher setting, Wang et al. (2020) build a multiplex graph network, Hu et al. (2020) aggregate features from a hierarchical decomposition, and Wu et al. (2020) apply a scattering transformation to learn objects, attributes, and relations. Recently, Zhang et al. (2021) employ a neuro-symbolic design but requires full knowledge over the hidden relations to perform *abduction*. While our work adopts the visual perception module and employs a similar training strategy from Zhang et al. (2021), the ALANS learner manages to *induce* the hidden relations without access to the ground-truth semantics of them, enabling the on-the-fly relation induction and systematic generalization on relational learning.

### 3 THE ALANS LEARNER

In this section, we introduce the ALANS learner for the RPM problem. In each RPM instance, an agent is given an incomplete  $3 \times 3$  panel matrix with the last entry missing and asked to induce the operator hidden in the matrix and choose from eight choice panels one that follows it. Formally, let the answer variable be denoted as  $y$ , the context panels as  $\{I_{o,i}\}_{i=1}^8$ , and choice panels as  $\{I_{c,i}\}_{i=1}^8$ . Then the problem can be formulated as estimating  $P(y \mid \{I_{o,i}\}_{i=1}^8, \{I_{c,i}\}_{i=1}^8)$ . According to the common design (Carpenter et al., 1990; Santoro et al., 2018; Zhang et al., 2019a), there is one operator that governs each panel attribute. Hence, by assuming independence among attributes, we propose to factorize the probability of  $P(y = n \mid \{I_{o,i}\}_{i=1}^8, \{I_{c,i}\}_{i=1}^8)$  as

$$\prod_a \sum_{\mathcal{T}^a} P(y^a = n \mid \mathcal{T}^a, \{I_{o,i}\}_{i=1}^8, \{I_{c,i}\}_{i=1}^8) \times P(\mathcal{T}^a \mid \{I_{o,i}\}_{i=1}^8), \quad (1)$$

where  $y^a$  denotes the answer selection based only on attribute  $a$  and  $\mathcal{T}^a$  the operator on  $a$ .

**Overview** As shown in Fig. 1, the ALANS learner decomposes the process into perception and reasoning: the neural visual perception frontend is adopted from (Zhang et al., 2021) and extracts the

*belief states* from each of the sixteen panels, whereas the algebraic abstract reasoning backend views an instance as an example in an abstract algebra structure, transforms belief states into *algebraic representation* by the representation theory, *induces* the hidden operators, and *executes* the operators to predict the representation of the answer. Therefore, in Eq. (1), the operator distribution is modeled by the fitness of an operator and the answer distribution by the distance between the predicted representation and that of a candidate.

### 3.1 NEURAL VISUAL PERCEPTION

We follow the design in Zhang et al. (2021) and decompose visual perception into an object CNN and a belief state inference engine. Specifically, for each panel, we use a sliding window to traverse the spatial domain of the image and feed each image region into an object CNN. The CNN has four branches, producing for each region its object attribute distributions, including objectiveness (if the region contains an object), type, size, and color. The belief inference engine summarizes the panel attribute distributions (over position, number, type, size, and color) by marginalizing out all object attribute distributions (over objectiveness, type, size, and color). As an example, the distribution of the panel attribute of Number can be computed as such: for  $N$  image regions and their predicted objectiveness

$$P(\text{Number} = k) = \sum_{\substack{R^o \in \{0,1\}^N \\ \sum_j R_j^o = k}} \prod_{j=1}^N P(r_j^o = R_j^o), \quad (2)$$

where  $P(r_j^o)$  denotes the  $j$ th region’s estimated objectiveness distribution, and  $R^o$  is a binary sequence of length  $N$  that sums to  $k$ . All panel attribute distributions compose the *belief state* of a panel. In the following, we denote the belief state as  $b$  and the distribution of an attribute  $a$  as  $P(b^a)$ . For more details, please refer to Zhang et al. (2021) and Appendix.

### 3.2 ALGEBRAIC ABSTRACT REASONING

Given the belief states of both context and choice panels, the algebraic abstract reasoning backend concerns the induction of hidden operators and the prediction of answer representation for each attribute. The fitness of induced operators is used for estimating the operator distribution and the difference between the prediction and the choice panel for estimating the answer distribution.

**Algebraic Underpinning** Without loss of generality, here we assume row-wise operators. For each attribute, under perfect perception, the first two rows in an RPM instance provide snapshots into an example of *group* (Hausmann & Ore, 1937) constrained to an integer-indexed set, a simple algebra structure that is closed under a binary operator. To see this, note that an accurate perception module would see each panel attribute as a deterministic set element. Therefore, RPM instances with unary operators, such as progression, are group examples with special binary operators where one operand is constant. Instances with binary operators, such as arithmetics, directly follow the group properties. Those with ternary operators are ones defined on a three-tuple set from rows.

**Algebraic Representation** A systematic algebraic view allows us to felicitously recruit ideas in the representation theory (Humphreys, 2012) to glean the hidden properties in the abstract structures: it makes abstract algebra amenable by reducing it onto linear algebra. Following the same spirit, we propose to lift both the set elements and the hidden operators to a learnable matrix space. To encode the set element, we employ the Peano Axiom (Peano, 1889). According to the Peano Axiom, an integer-indexed set can be constructed by (1) a zero element ( $\mathbf{0}$ ), (2) a successor function ( $S(\cdot)$ ), and (3) the principle of mathematical induction, such that the  $k$ th element is encoded as  $S^k(\mathbf{0})$ . Specifically, we instantiate the zero element as a learnable matrix  $M_0$  and the successor function as the matrix-matrix product parameterized by  $M$ . In an attribute-specific manner,

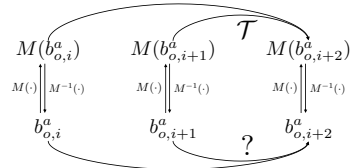


Figure 2: Isomorphism between the abstract algebra and the matrix-based representation. Operator induction is now reduced to solving for a matrix.

the representation of an attribute taking the  $k$ th value is  $(M^a)^k M_0^a$ . For operators, we consider them to live in a learnable matrix group of a corresponding dimension, such that the action of an operator on a set can be represented as matrix multiplication. Such algebraic representation establishes an isomorphism between the matrix space and the abstract algebraic structure: abstract elements on the algebraic structure have a bijective mapping to/from the matrix space, and inducing the abstract relation can be reduced to solving for a matrix operator. See Fig. 2 for a graphical illustration of the isomorphism.

**Operator Induction** Operator induction concerns about finding a concrete operator in the abstract algebraic structure. By the property of closure, we formulate it as an inner-level regularized linear regression problem: a binary operator  $\mathcal{T}_b^a$  in a group example for attribute  $a$  minimizes  $\arg \min_{\mathcal{T}} \ell_b^a(\mathcal{T})$  defined as

$$\ell_b^a(\mathcal{T}) = \sum_i \mathbb{E} [\|M(b_{o,i}^a) \mathcal{T} M(b_{o,i+1}^a) - M(b_{o,i+2}^a)\|_F^2] + \lambda_b^a \|\mathcal{T}\|_F^2, \quad (3)$$

where under visual uncertainty, we take the expectation with respect to the distributions in the belief states of context panels  $P(b_{o,i}^a)$  in the first two rows, and denote its algebraic representation as  $M(b_{o,i}^a)$ . For unary operators, one operand can be treated as constant and absorbed into  $\mathcal{T}$ . Note that Eq. (3) admits a closed-form solution (see Appendix for details). Therefore, the operator can be learned and adapted for different instances of binary relations and concluded on the fly. Such a design also simplifies the recent neuro-symbolic approaches, where every single symbol operator needs to be hand-defined (Han et al., 2019; Mao et al., 2019; Yi et al., 2020; 2018). Instead, we only specify an inner-level optimization framework and allow symbolic operators to be quickly induced based on the neural observations, while keeping the semantic interpretability in the neuro-symbolic methods. Therefore, we term such a design semi-symbolic.

The operator probability in Eq. (1) is then modeled by each operator type’s fitness, *e.g.*, for binary,

$$P(\mathcal{T}^a = \mathcal{T}_b^a \mid \{I_{o,i}\}_{i=1}^8) \propto \exp(-\ell_b^a(\mathcal{T}_b^a)). \quad (4)$$

**Operator Execution** To predict the algebraic representation of the answer, we solve another inner-level optimization similar to Eq. (3), but now treating the representation of the answer as a variable:

$$\widehat{M}_b^a = \arg \min_M \ell_b^a(M) = \mathbb{E}[\|M(b_{o,7}^a) \mathcal{T}_b^a M(b_{o,8}^a) - M\|_F^2], \quad (5)$$

where the expectation is taken with respect to context panels in the last row. The optimization also admits a closed-form solution (see Appendix for details), which corresponds to the execution of the induced operator in Eq. (3).

The predicted representation is decoded probabilistically as the predicted belief state of the solution,

$$P(\widehat{b}^a = k \mid \mathcal{T}^a) \propto \exp(-\|\widehat{M}^a - (M^a)^k M_0^a\|_F^2). \quad (6)$$

**Answer Selection** Based on Eqs. (1) and (4), estimating the answer distribution is now boiled down to estimating the conditional answer distributions for each attribute. Here, we propose to model it based on the Jensen–Shannon Divergence (JSD) of the predicted belief state and that of a choice,

$$P(y^a = n \mid \mathcal{T}^a, \{I_{o,i}\}_{i=1}^8, \{I_{c,i}\}_{i=1}^8) \propto \exp(-d_n^a), \quad (7)$$

where we define  $d_n^a$  as

$$d_n^a = \mathbb{D}_{\text{JSD}}(P(\widehat{b}^a \mid \mathcal{T}^a) \parallel P(b_{c,n}^a)). \quad (8)$$

We also note that by decoding the predicted representation in Eq. (6), a solution can be *generated*: by sequentially selecting the most probable operator and the most probable attribute value, a rendering engine can directly render the solution. The reasoning backend also enables end-to-end training: by integrating the belief states from neural perception, the module conducts both induction and execution in a soft manner, such that the gradients can be back-propagated and both the visual frontend and the reasoning backend jointly trained.

### 3.3 TRAINING STRATEGY

We train the entire ALANS learner by minimizing the cross-entropy loss between the estimated answer distribution and the ground-truth selection and an auxiliary loss (Santoro et al., 2018; Wang et al., 2020; Zhang et al., 2019a; 2021) that shapes the operator distribution from the reasoning engine, *i.e.*,

$$\min_{\theta, \{M_0^a\}, \{M^a\}} \ell(P(y \mid \{I_{o,i}\}_{i=1}^8, \{I_{c,i}\}_{i=1}^8), y_\star) + \sum_a \lambda^a \ell(P(\mathcal{T}^a \mid \{I_{o,i}\}_{i=1}^8), y_\star^a), \quad (9)$$

where  $\ell(\cdot)$  denotes the cross-entropy loss,  $y_\star$  the correct choice in candidates, and  $y_\star^a$  the ground-truth operator selection for attribute  $a$ , respectively. The first part of the loss encourages the model to select the right choice for evaluation, while the second part motivates meaningful internal representation to emerge. Compared to Zhang et al. (2021), the system requires joint operation from not only a trained perception module  $\theta$ , but also the algebraic encodings from the zero elements and the successor function  $\{M_0^a\}$  and  $\{M^a\}$ , and correspondingly, the induced operator  $\mathcal{T}$ . We notice the three-stage curriculum in Zhang et al. (2021) is crucial for such a neuro-semi-symbolic system. In particular, we use  $\lambda^a$  to balance the trade-off in the curriculum: in the first stage, we only train parameters regarding objectiveness; in the second stage, we freeze objectiveness parameters and cyclically train parameters involving type, size, and color; in the last stage, we fine-tune all parameters.

## 4 EXPERIMENTS

A cognitive architecture with systematic generalization is believed to demonstrate the following three principles (Fodor et al., 1988; Marcus, 2001; 2020): (1) systematicity, (2) productivity, and (3) localism. Systematicity requires an architecture to be able to entertain “semantically related” contents after understanding a given thought. Productivity states the awareness of a constituent implies that of a recursive application of the constituent; vice versa for localism.

To verify the effectiveness of an algebraic treatment in systematic generalization, we showcase the superiority of the proposed ALANS learner on the three principles in the abstract spatial-temporal reasoning task of RPM. Specifically, we use the generation methods proposed in Zhang et al. (2019a) and Hu et al. (2020) to generate RPM problems and carefully split training and testing to construct the three regimes. The former generates candidates by perturbing only one attribute of the correct answer while the later modifies attribute values in a hierarchical manner to avoid shortcut solutions by pure statistics. Both methods categorize relations in RPM into three types, according to Carpenter et al. (1990): unary (Constant and Progression), binary (Arithmetic), and ternary (Distribution of Three), each of which comes with several instances. Grounding the principles into learning abstract relations in RPM, we fix the configuration to be  $3 \times 3$ Grid and generate the following data splits for evaluation (see Appendix for details and in-distribution results):

- Systematicity: the training set contains only a subset of instances for each type of relation, while the test set all other relation instances.
- Productivity: as the binary relation results from a recursive application of the unary relation, the training set contains only unary relations, whereas the test set only binary relations.
- Localism: the training and testing sets in the productivity split are swapped to study localism.

We follow Zhang et al. (2019a) to generate 10,000 instances for each split.

### 4.1 EXPERIMENTAL SETUP

We evaluate the systematic generalizability of the proposed ALANS learner on the above three splits, and compare the ALANS learner with other baselines, including ResNet, ResNet+DRT (Zhang et al., 2019a), WReN (Santoro et al., 2018), CoPINet (Zhang et al., 2019b), MXGNet (Wang et al., 2020), LEN (Zheng et al., 2019), HriNet (Hu et al., 2020), and SCL (Wu et al., 2020). We use either official or public implementations that reproduce the original results. All models are implemented in PyTorch (Paszke et al., 2017) and optimized using ADAM (Kingma & Ba, 2014) on an Nvidia Titan Xp GPU. We validate trained models on validation sets and report performance on test sets.

Table 1: Model performance on different aspects of systematic generalization. The performance is measured by accuracy on the test sets. Upper: results on datasets generated by Zhang et al. (2019a). Lower: results on datasets generated by Hu et al. (2020).

Method	MXGNet	ResNet+DRT	ResNet	HriNet	LEN	WReN	SCL	CoPINet	ALANS	ALANS-Ind	ALANS-GT
Systematicity	20.95%	33.00%	27.35%	28.05%	40.15%	35.20%	37.35%	59.30%	<b>78.45%</b>	52.70%	93.85%
Productivity	30.40%	27.95%	27.05%	31.45%	42.30%	56.95%	51.10%	60.00%	<b>79.95%</b>	36.45%	90.20%
Localism	28.80%	24.90%	23.05%	29.70%	39.65%	38.70%	47.75%	60.10%	<b>80.50%</b>	59.80%	95.30%
Average	26.72%	28.62%	25.82%	29.73%	40.70%	43.62%	45.40%	59.80%	<b>79.63%</b>	48.65%	93.12%
Systematicity	13.35%	13.50%	14.20%	21.00%	17.40%	15.00%	24.90%	18.35%	<b>64.80%</b>	52.80%	84.85%
Productivity	14.10%	16.10%	20.70%	20.35%	19.70%	17.95%	22.20%	29.10%	<b>65.55%</b>	32.10%	86.55%
Localism	15.80%	13.85%	17.45%	24.60%	20.15%	19.70%	29.95%	31.85%	<b>65.90%</b>	50.70%	90.95%
Average	14.42%	14.48%	17.45%	21.98%	19.08%	17.55%	25.68%	26.43%	<b>65.42%</b>	45.20%	87.45%

Table 2: Perception accuracy of the proposed ALANS learner, measured by whether the module can correctly predict an attribute’s value. Left: results on datasets generated by Zhang et al. (2019a). Right: results on datasets generated by Hu et al. (2020).

Object Attribute	Objectiveness	Type	Size	Color	Object Attribute	Objectiveness	Type	Size	Color
Systematicity	100.00%	99.95%	94.65%	71.35%	Systematicity	100.00%	96.34%	92.36%	63.98%
Productivity	100.00%	99.97%	98.04%	77.61%	Productivity	100.00%	94.28%	97.00%	69.89%
Localism	100.00%	95.65%	98.56%	80.05%	Localism	100.00%	95.80%	98.36%	60.35%
Average	100.00%	98.52%	97.08%	76.34%	Average	100.00%	95.47%	95.91%	64.74%

Table 3: Reasoning accuracy of the proposed ALANS learner, measured by whether the module can correctly predict the type of a relation on an attribute. Left: results on datasets generated by Zhang et al. (2019a). Right: results on datasets generated by Hu et al. (2020).

Relation on	Position	Number	Type	Size	Color	Relation on	Position	Number	Type	Size	Color
Systematicity	72.04%	82.14%	81.50%	80.80%	40.40%	Systematicity	69.96%	80.34%	83.50%	80.85%	28.85%
Productivity	-	98.75%	89.50%	72.10%	33.95%	Productivity	-	99.10%	87.95%	68.50%	23.10%
Localism	-	74.70%	44.25%	56.40%	54.20%	Localism	-	70.55%	36.65%	42.30%	33.20%
Average	72.04%	85.20%	71.75%	69.77%	42.85%	Average	69.96%	83.33%	69.37%	63.88%	28.38%

## 4.2 SYSTEMATIC GENERALIZATION

Table 1 shows the performance of various models on systematic generalization, *i.e.*, systematicity, productivity, and localism. Compared to results reported in (Hu et al., 2020; Santoro et al., 2018; Wang et al., 2020; Wu et al., 2020; Zhang et al., 2019a;b; Zheng et al., 2019), all pure connectionist models experience a devastating performance drop when it comes to the critical cognitive requirements on systematic generalization, indicating that pure connectionist models fail to perform abstraction, algebraization, induction, or generalization needed in solving the abstract reasoning task; instead, they seem to only take a shortcut to bypass them. In particular, MXGNet’s (Wang et al., 2020) superiority is diminishing in systematic generalization. In spite of learning with structural annotations, ResNet+DRT (Zhang et al., 2019a) does not fare better than its base model. The recently proposed HriNet (Hu et al., 2020) slightly improves on ResNet in this aspect, with LEN (Zheng et al., 2019) being only marginally better. WReN (Santoro et al., 2018), on the other hand, shows oscillating performance across the three regimes. Evaluated under systematic generation, SCL (Wu et al., 2020) and CoPINet (Zhang et al., 2019b) also far deviate from their “superior performance”. These observations suggest that pure connectionist models highly likely learn from variation in visual appearance rather than the algebra underlying the problem.

Embedded in a neural-semi-symbolic framework, the proposed ALANS learner improves on systematic generalization by a large margin. With an algebra-aware design, the model is considerably stable across different principles of systematic generalization. The algebraic representation learned in relations of either a constituent or a recursive composition naturally supports productivity and localism, while semi-symbolic inner optimization further allows various instances of an operator type to be induced from the algebraic representation and boosts systematicity. The importance of the algebraic representation is made more significant in the ablation study: ALANS-Ind, with algebraic representation replaced by independent encodings and the algebraic isomorphism broken, shows inferior performance. We also examine the model’s performance under perfect perception (denoted as ALANS-GT) to see how the proposed algebraic reasoning module works: the gap from perfection indicates space for improvement for the inductive reasoning part of the model. In the next section, we further show that the neuro-semi-symbolic decomposition in ALANS’s design enables diagnostic tests into its jointly learned perception module and reasoning module. This design is in stark contrast to black-box models.



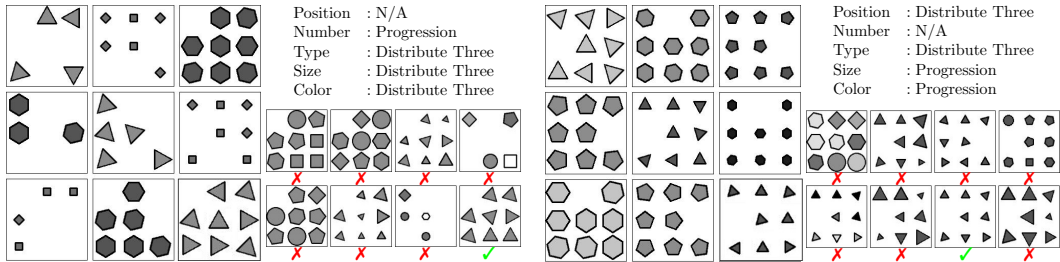


Figure 3: Examples of RPM instances with the missing entries filled by solutions generated by the ALANS learner. Ground-truth relations are also listed. Note the generated results do not look exactly like the correct choices due to random rotations during rendering, but are semantically correct.

### 4.3 ANALYSIS INTO PERCEPTION AND REASONING

The neural-semi-symbolic design allows analyses into both perception and reasoning. To evaluate the neural perception module and the algebraic reasoning module, we extract region-based object attribute annotations from the dataset generation methods (Hu et al., 2020; Zhang et al., 2019a) and categorize all relations into three types, *i.e.*, unary, binary, and ternary, respectively.

Table 2 shows the perception module’s performance on the test sets in the three regimes of systematic generalization. We note that in order for the ALANS learner to achieve the desired results shown in Table 1, ALANS learns to construct the concept of objectiveness perfectly. The model also shows fairly accurate prediction on the attributes of type and size. However, on the texture-related concept of color, ALANS fails to develop a reliable notion on it. Despite that, the general prediction accuracy of the perception module is still surprising, considering that the perception module is jointly learned with ground-truth annotations on answer selections. The relatively lower accuracy on color could be attributed to its larger space compared to other attributes.

Table 3 lists the reasoning module’s performance during testing for the three aspects. Note that on position, the unary operator (shifting) and binary operator (set arithmetics) do not systematically imply each other. Hence, we do not count them as probes into productivity and localism. In general, we notice that the better the perception accuracy on one attribute, the better the performance on reasoning. However, we also note that despite the relatively accurate perception of objectiveness, type, and size, near perfect reasoning is never guaranteed. This deficiency is due to the perception uncertainty handled by expectation in Eq. (3): in spite of correctness when we take  $\arg \max$ , marginalizing by expectation will unavoidably introduce noise into the reasoning process. Therefore, an ideal reasoning module requires the perception frontend to be not only correct but also certain. Computationally, one can sample from the perception module and optimize Eq. (9) using REINFORCE (Williams, 1992). However, the credit assignment problem and variance in gradient estimation will further complicate training.

### 4.4 GENERATIVE POTENTIAL

Compared to existing discriminative-only RPM-solving methods, the proposed ALANS learner is unique in its generative potential. As mentioned above, the final panel attribute can be decoded by sequentially selecting the most probable hidden operator and the attribute value. When equipped with a rendering engine, a solution can be generated. In Fig. 3, we use the rendering program from Zhang et al. (2019a) to demonstrate such a generative potential in the proposed ALANS learner.

## 5 CONCLUSION

In this work, we propose the ALgebra-Aware Neuro-Semi-Symbolic (ALANS) learner, echoing a normative theory in the connectionist-classicist debate that an algebraic treatment in a cognitive architecture should improve a model’s systematic generalization ability. Compared to earlier works, the ALANS learner employs a neural-semi-symbolic architecture, where the algebraic abstract reasoning module transforms visual information into algebraic representation with isomorphism established by the Peano Axiom and the representation theory, conducts operator induction, and executes it to arrive at an answer. In three RPM domains reflective of systematic generalization, the proposed ALANS learner shows superior performance compared to other pure connectionist baselines.

## REFERENCES

- Saint Augustine. *The confessions*. Clark, 1876.
- Dzmitry Bahdanau, Shikhar Murty, Michael Noukhovitch, Thien Huu Nguyen, Harm de Vries, and Aaron Courville. Systematic generalization: What is required and can it be learned? In *International Conference on Learning Representations (ICLR)*, 2019.
- Jonathan F Bard. *Practical bilevel optimization: algorithms and applications*, volume 30. Springer Science & Business Media, 2013.
- Patricia A Carpenter, Marcel A Just, and Peter Shell. What one intelligence test measures: a theoretical account of the processing in the raven progressive matrices test. *Psychological Review*, 97(3):404, 1990.
- Xinyun Chen, Chen Liang, Adams Wei Yu, Dawn Song, and Denny Zhou. Compositional generalization via neural-symbolic stack machines. *arXiv preprint arXiv:2008.06662*, 2020.
- Zhenfang Chen, Jiayuan Mao, Jiajun Wu, Kwan-Yee Kenneth Wong, Joshua B Tenenbaum, and Chuang Gan. Grounding physical concepts of objects and events through dynamic visual reasoning. *arXiv preprint arXiv:2103.16564*, 2021.
- François Chollet. The measure of intelligence. *arXiv preprint arXiv:1911.01547*, 2019.
- Benoît Colson, Patrice Marcotte, and Gilles Savard. An overview of bilevel optimization. *Annals of operations research*, 153(1):235–256, 2007.
- Honghua Dong, Jiayuan Mao, Tian Lin, Chong Wang, Lihong Li, and Denny Zhou. Neural logic machines. *arXiv preprint arXiv:1904.11694*, 2019.
- Richard Evans and Edward Grefenstette. Learning explanatory rules from noisy data. *Journal of Artificial Intelligence Research*, 61:1–64, 2018.
- Jerry Fodor and Brian P McLaughlin. Connectionism and the problem of systematicity: Why smolensky’s solution doesn’t work. *Cognition*, 35(2):183–204, 1990.
- Jerry A Fodor. *The language of thought*, volume 5. Harvard university press, 1975.
- Jerry A Fodor, Zenon W Pylyshyn, et al. Connectionism and cognitive architecture: A critical analysis. *Cognition*, 28(1-2):3–71, 1988.
- Artur S d’Avila Garcez, Krysia B Broda, and Dov M Gabbay. *Neural-symbolic learning systems: foundations and applications*. Springer Science & Business Media, 2012.
- Chi Han, Jiayuan Mao, Chuang Gan, Josh Tenenbaum, and Jiajun Wu. Visual concept-metaconcept learning. In *Proceedings of Advances in Neural Information Processing Systems (NeurIPS)*, 2019.
- Bernard A Hausmann and Oystein Ore. Theory of quasi-groups. *American Journal of Mathematics*, 59(4):983–1004, 1937.
- Thomas Little Heath et al. *The thirteen books of Euclid’s Elements*. Courier Corporation, 1956.
- Felix Hill, Adam Santoro, David GT Barrett, Ari S Morcos, and Timothy Lillicrap. Learning to make analogies by contrasting abstract relational structure. In *International Conference on Learning Representations (ICLR)*, 2019.
- Douglas R Hofstadter. *Fluid concepts and creative analogies: Computer models of the fundamental mechanisms of thought*. Basic books, 1995.
- Sheng Hu, Yuqing Ma, Xianglong Liu, Yanlu Wei, and Shihao Bai. Hierarchical rule induction network for abstract visual reasoning. *arXiv preprint arXiv:2002.06838*, 2020.
- Drew A Hudson and Christopher D Manning. Learning by abstraction: The neural state machine. *arXiv preprint arXiv:1907.03950*, 2019.

- James E Humphreys. *Introduction to Lie algebras and representation theory*, volume 9. Springer Science & Business Media, 2012.
- Susanne M Jaeggi, Martin Buschkuhl, John Jonides, and Walter J Perrig. Improving fluid intelligence with training on working memory. *Proceedings of the National Academy of Sciences*, 105(19):6829–6833, 2008.
- William James. *The Principles of Psychology*. Henry Holt and Company, 1891.
- Ken Kansky, Tom Silver, David A Mély, Mohamed Eldawy, Miguel Lázaro-Gredilla, Xinghua Lou, Nimrod Dorfman, Szymon Sidor, Scott Phoenix, and Dileep George. Schema networks: Zero-shot transfer with a generative causal model of intuitive physics. In *Proceedings of International Conference on Machine Learning (ICML)*, 2017.
- Diederik P Kingma and Jimmy Ba. Adam: A method for stochastic optimization. In *International Conference on Learning Representations (ICLR)*, 2014.
- Diederik P Kingma and Max Welling. Auto-encoding variational bayes. *arXiv preprint arXiv:1312.6114*, 2013.
- Brenden Lake and Marco Baroni. Generalization without systematicity: On the compositional skills of sequence-to-sequence recurrent networks. In *Proceedings of International Conference on Machine Learning (ICML)*, 2018.
- Peter Lancaster. Explicit solutions of linear matrix equations. *SIAM review*, 12(4):544–566, 1970.
- Yann LeCun, Léon Bottou, Yoshua Bengio, Patrick Haffner, et al. Gradient-based learning applied to document recognition. *Proceedings of the IEEE*, 86(11):2278–2324, 1998.
- Daniel R Little, Stephan Lewandowsky, and Thomas L Griffiths. A bayesian model of rule induction in raven’s progressive matrices. In *Proceedings of the Annual Meeting of the Cognitive Science Society (CogSci)*, 2012.
- Andrew Lovett and Kenneth Forbus. Modeling visual problem solving as analogical reasoning. *Psychological Review*, 124(1):60, 2017.
- Andrew Lovett, Emmett Tomai, Kenneth Forbus, and Jeffrey Usher. Solving geometric analogy problems through two-stage analogical mapping. *Cognitive Science*, 33(7):1192–1231, 2009.
- Andrew Lovett, Kenneth Forbus, and Jeffrey Usher. A structure-mapping model of raven’s progressive matrices. In *Proceedings of the Annual Meeting of the Cognitive Science Society (CogSci)*, 2010.
- Penelope Maddy. Believing the axioms. i. *The Journal of Symbolic Logic*, 53(2):481–511, 1988.
- Robin Manhaeve, Sebastijan Dumancic, Angelika Kimmig, Thomas Demeester, and Luc De Raedt. Deepproblog: Neural probabilistic logic programming. In *Advances in Neural Information Processing Systems*, pp. 3749–3759, 2018.
- Jiayuan Mao, Chuang Gan, Pushmeet Kohli, Joshua B Tenenbaum, and Jiajun Wu. The neuro-symbolic concept learner: Interpreting scenes, words, and sentences from natural supervision. In *International Conference on Learning Representations (ICLR)*, 2019.
- Gary Marcus. *The algebraic mind*. Cambridge, MA: MIT Press, 2001.
- Gary Marcus. The next decade in ai: four steps towards robust artificial intelligence. *arXiv preprint arXiv:2002.06177*, 2020.
- Gary F Marcus, Sugumaran Vijayan, S Bandi Rao, and Peter M Vishton. Rule learning by seven-month-old infants. *Science*, 283(5398):77–80, 1999.
- John McCarthy. *Programs with common sense*. RLE and MIT computation center, 1960.
- Keith McGreggor and Ashok Goel. Confident reasoning on raven’s progressive matrices tests. In *Proceedings of AAAI Conference on Artificial Intelligence (AAAI)*, 2014.

- Keith McGregor, Maithilee Kunda, and Ashok Goel. Fractals and ravens. *Artificial Intelligence*, 215:1–23, 2014.
- Can Serif Mekik, Ron Sun, and David Yun Dai. Similarity-based reasoning, raven’s matrices, and general intelligence. In *Proceedings of International Joint Conference on Artificial Intelligence (IJCAI)*, 2018.
- Allen Newell. Physical symbol systems. *Cognitive science*, 4(2):135–183, 1980.
- Adam Paszke, Sam Gross, Soumith Chintala, Gregory Chanan, Edward Yang, Zachary DeVito, Zeming Lin, Alban Desmaison, Luca Antiga, and Adam Lerer. Automatic differentiation in PyTorch. In *NIPS Autodiff Workshop*, 2017.
- Giuseppe Peano. *Arithmetices principia: Nova methodo exposita*. Fratres Bocca, 1889.
- James C Raven. Mental tests used in genetic studies: The performance of related individuals on tests mainly educative and mainly reproductive. Master’s thesis, University of London, 1936.
- John C Raven and John Hugh Court. *Raven’s progressive matrices and vocabulary scales*. Oxford psychologists Press, 1998.
- Tim Rocktäschel and Sebastian Riedel. End-to-end differentiable proving. In *Advances in Neural Information Processing Systems*, pp. 3788–3800, 2017.
- Adam Santoro, David Raposo, David G Barrett, Mateusz Malinowski, Razvan Pascanu, Peter Battaglia, and Timothy Lillicrap. A simple neural network module for relational reasoning. In *Proceedings of Advances in Neural Information Processing Systems (NeurIPS)*, 2017.
- Adam Santoro, Felix Hill, David Barrett, Ari Morcos, and Timothy Lillicrap. Measuring abstract reasoning in neural networks. In *Proceedings of International Conference on Machine Learning (ICML)*, 2018.
- Luciano Serafini and Artur d’Avila Garcez. Logic tensor networks: Deep learning and logical reasoning from data and knowledge. *arXiv preprint arXiv:1606.04422*, 2016.
- Snejana Shegheva and Ashok Goel. The structural affinity method for solving the raven’s progressive matrices test for intelligence. In *Proceedings of AAAI Conference on Artificial Intelligence (AAAI)*, 2018.
- Charles Spearman. *The nature of “intelligence” and the principles of cognition*. Macmillan, 1923.
- Charles Spearman. *The abilities of man*, volume 6. Macmillan New York, 1927.
- Xander Steenbrugge, Sam Leroux, Tim Verbelen, and Bart Dhoedt. Improving generalization for abstract reasoning tasks using disentangled feature representations. *arXiv preprint arXiv:1811.04784*, 2018.
- Duo Wang, Mateja Jamnik, and Pietro Lio. Abstract diagrammatic reasoning with multiplex graph networks. In *International Conference on Learning Representations (ICLR)*, 2020.
- Ke Wang and Zhendong Su. Automatic generation of raven’s progressive matrices. In *Proceedings of International Joint Conference on Artificial Intelligence (IJCAI)*, 2015.
- Ronald J Williams. Simple statistical gradient-following algorithms for connectionist reinforcement learning. *Machine learning*, 8(3-4):229–256, 1992.
- Terry Winograd. Procedures as a representation for data in a computer program for understanding natural language. Technical report, MIT. Cent. Space Res., 1971.
- Ludwig Wittgenstein. *Philosophical investigations. Philosophische Untersuchungen*. Macmillan, 1953.
- Jiajun Wu, Joshua B Tenenbaum, and Pushmeet Kohli. Neural scene de-rendering. In *Proceedings of the IEEE Conference on Computer Vision and Pattern Recognition (CVPR)*, 2017.

- Yuhuai Wu, Honghua Dong, Roger Grosse, and Jimmy Ba. The scattering compositional learner: Discovering objects, attributes, relationships in analogical reasoning. *arXiv preprint arXiv:2007.04212*, 2020.
- Kexin Yi, Jiajun Wu, Chuang Gan, Antonio Torralba, Pushmeet Kohli, and Josh Tenenbaum. Neural-symbolic vqa: Disentangling reasoning from vision and language understanding. In *Proceedings of Advances in Neural Information Processing Systems (NeurIPS)*, 2018.
- Kexin Yi, Chuang Gan, Yunzhu Li, Pushmeet Kohli, Jiajun Wu, Antonio Torralba, and Joshua Tenenbaum. Clevrer: Collision events for video representation and reasoning. In *International Conference on Learning Representations (ICLR)*, 2020.
- Chi Zhang, Feng Gao, Baoxiong Jia, Yixin Zhu, and Song-Chun Zhu. Raven: A dataset for relational and analogical visual reasoning. In *Proceedings of the IEEE Conference on Computer Vision and Pattern Recognition (CVPR)*, 2019a.
- Chi Zhang, Baoxiong Jia, Feng Gao, Yixin Zhu, Hongjing Lu, and Song-Chun Zhu. Learning perceptual inference by contrasting. In *Proceedings of Advances in Neural Information Processing Systems (NeurIPS)*, 2019b.
- Chi Zhang, Baoxiong Jia, Song-Chun Zhu, and Yixin Zhu. Abstract spatial-temporal reasoning via probabilistic abduction and execution. In *Proceedings of the IEEE Conference on Computer Vision and Pattern Recognition (CVPR)*, 2021.
- Kecheng Zheng, Zheng-Jun Zha, and Wei Wei. Abstract reasoning with distracting features. In *Proceedings of Advances in Neural Information Processing Systems (NeurIPS)*, 2019.
- Song-Chun Zhu, David Mumford, et al. A stochastic grammar of images. *Foundations and Trends® in Computer Graphics and Vision*, 2(4):259–362, 2007.

## A INDUCING AND EXECUTING OPERATORS

In the main text, we exemplify the induction and the execution process using a binary operator. Here, we discuss other details regarding the formulation for all three types of operators, *i.e.*, unary, binary, and ternary.

**Unary Operator** To induce the unary operator  $\mathcal{T}_u^a$  for an attribute  $a$ , we solve the following optimization problem

$$\mathcal{T}_u^a = \arg \min_{\mathcal{T}} \ell_u^a(\mathcal{T}), \quad (\text{S1})$$

where

$$\begin{aligned} \ell_u^a(\mathcal{T}) = 1/5 \times & \left( \mathbb{E} \left[ \|M(b_{o,1}^a)\mathcal{T} - M(b_{o,2}^a)\|_F^2 \right] + \right. \\ & \mathbb{E} \left[ \|M(b_{o,2}^a)\mathcal{T} - M(b_{o,3}^a)\|_F^2 \right] + \\ & \mathbb{E} \left[ \|M(b_{o,4}^a)\mathcal{T} - M(b_{o,5}^a)\|_F^2 \right] + \\ & \mathbb{E} \left[ \|M(b_{o,5}^a)\mathcal{T} - M(b_{o,6}^a)\|_F^2 \right] + \\ & \left. \mathbb{E} \left[ \|M(b_{o,7}^a)\mathcal{T} - M(b_{o,8}^a)\|_F^2 \right] \right) + \\ & \lambda_u^a \|\mathcal{T}\|_F^2. \end{aligned} \quad (\text{S2})$$

The indexing follows the row / column major. By taking the derivative with respect to  $\mathcal{T}$  and setting it to be  $\mathbf{0}$ , we have the following solution,

$$\mathcal{T}_u^a = A^{-1}B \quad (\text{S3})$$

where, assuming independence,

$$\begin{aligned} A = & \mathbb{E} [M(b_{o,1}^a)^T M(b_{o,1}^a)] + \mathbb{E} [M(b_{o,2}^a)^T M(b_{o,2}^a)] + \\ & \mathbb{E} [M(b_{o,4}^a)^T M(b_{o,4}^a)] + \mathbb{E} [M(b_{o,5}^a)^T M(b_{o,5}^a)] + \\ & \mathbb{E} [M(b_{o,7}^a)^T M(b_{o,7}^a)] + 5\lambda_u^a I \end{aligned} \quad (\text{S4})$$

and

$$\begin{aligned} B = & \mathbb{E} [M(b_{o,1}^a)^T] \mathbb{E} [M(b_{o,2}^a)] + \\ & \mathbb{E} [M(b_{o,2}^a)^T] \mathbb{E} [M(b_{o,3}^a)] + \\ & \mathbb{E} [M(b_{o,4}^a)^T] \mathbb{E} [M(b_{o,5}^a)] + \\ & \mathbb{E} [M(b_{o,5}^a)^T] \mathbb{E} [M(b_{o,6}^a)] + \\ & \mathbb{E} [M(b_{o,7}^a)^T] \mathbb{E} [M(b_{o,8}^a)]. \end{aligned} \quad (\text{S5})$$

Note that as long as  $\lambda_u^a > 0$ ,  $A$  is a symmetric positive definite matrix and hence is invertible. Compared to the binary case, the unary operator can be regarded as a special binary operator where one of the operand is a constant, absorbed into operator learning, and jointly solved.

To predict the answer representation, we solve another optimization problem, *i.e.*,

$$\widehat{M}_u^a = \arg \min_M \ell_u^a(M) = \mathbb{E} \left[ \|M(b_{o,8}^a)\mathcal{T}_u^a - M\|_F^2 \right]. \quad (\text{S6})$$

Taking its derivative and setting it to  $\mathbf{0}$ , we have

$$\widehat{M}_u^a = \mathbb{E} [M(b_{o,8}^a)] \mathcal{T}_u^a. \quad (\text{S7})$$

Note that this is exactly the execution of the learned operator.

**Binary Operator** The optimization problem for the binary case can be formulated as

$$\mathcal{T}_b^a = \arg \min_{\mathcal{T}} \ell_b^a(\mathcal{T}), \quad (\text{S8})$$

where

$$\begin{aligned} \ell_b^a(\mathcal{T}) = & 1/2 \times \left( \mathbb{E} \left[ \|M(b_{o,1}^a) \mathcal{T} M(b_{o,2}^a) - M(b_{o,3}^a)\|_F^2 \right] + \right. \\ & \left. \mathbb{E} \left[ \|M(b_{o,4}^a) \mathcal{T} M(b_{o,5}^a) - M(b_{o,6}^a)\|_F^2 \right] \right) + \\ & \lambda_b^a \|\mathcal{T}\|_F^2. \end{aligned} \quad (\text{S9})$$

We note that, assuming independence, the solution satisfies

$$\begin{aligned} & \mathbb{E} [M(b_{o,1}^a)^T M(b_{o,1}^a)] \mathcal{T} \mathbb{E} [M(b_{o,2}^a) M(b_{o,2}^a)^T] + \\ & \mathbb{E} [M(b_{o,4}^a)^T M(b_{o,4}^a)] \mathcal{T} \mathbb{E} [M(b_{o,5}^a) M(b_{o,5}^a)^T] + 2\lambda_b^a \mathcal{T} \\ = & \mathbb{E} [M(b_{o,1}^a)^T] \mathbb{E} [M(b_{o,3}^a)] \mathbb{E} [M(b_{o,2}^a)^T] + \\ & \mathbb{E} [M(b_{o,4}^a)^T] \mathbb{E} [M(b_{o,6}^a)] \mathbb{E} [M(b_{o,5}^a)^T]. \end{aligned} \quad (\text{S10})$$

This is a linear matrix equation and can be turned into a linear equation by vectorization. Using  $\text{vec}(A\mathcal{T}B) = A \otimes B \text{vec}(\mathcal{T})$  (Lancaster, 1970), where  $\otimes$  denotes the Kronecker product, we have

$$\text{vec}(\mathcal{T}_b^a) = A^{-1}B, \quad (\text{S11})$$

where

$$\begin{aligned} A = & \mathbb{E} [M(b_{o,1}^a)^T M(b_{o,1}^a)] \otimes \mathbb{E} [M(b_{o,2}^a) M(b_{o,2}^a)^T] + \\ & \mathbb{E} [M(b_{o,4}^a)^T M(b_{o,4}^a)] \otimes \mathbb{E} [M(b_{o,5}^a) M(b_{o,5}^a)^T] + \\ & 2\lambda_b^a I \end{aligned} \quad (\text{S12})$$

and

$$\begin{aligned} B = & \text{vec} \left( \mathbb{E} [M(b_{o,1}^a)^T] \mathbb{E} [M(b_{o,3}^a)] \mathbb{E} [M(b_{o,2}^a)^T] \right) + \\ & \text{vec} \left( \mathbb{E} [M(b_{o,4}^a)^T] \mathbb{E} [M(b_{o,6}^a)] \mathbb{E} [M(b_{o,5}^a)^T] \right). \end{aligned} \quad (\text{S13})$$

Note that  $A$  is also symmetric positive definite given positive  $\lambda_b^a$  and hence invertible.

The predicted answer representation is given by

$$\widehat{M}_b^a = \arg \min_M \ell_b^a(M) = \mathbb{E} \left[ \|M(b_{o,7}^a) \mathcal{T}_b^a M(b_{o,8}^a) - M\|_F^2 \right], \quad (\text{S14})$$

which can be solved by executing the induced binary operator  $\widehat{M}_b^a = \mathbb{E} [M(b_{o,7}^a)] \mathcal{T}_b^a \mathbb{E} [M(b_{o,8}^a)]$ .

**Ternary Operator** A ternary operation can be regarded as a unary operation on elements defined on rows / columns. Specifically, we propose to construct the algebraic representation of a row / column by concatenating the algebraic representation of each panel in it, *i.e.*,

$$M(b_{o,i}^a, b_{o,i+1}^a, b_{o,i+2}^a) = [M(b_{o,i}^a); M(b_{o,i+1}^a); M(b_{o,i+2}^a)]. \quad (\text{S15})$$

Then the ternary operator can be solved by

$$\mathcal{T}_t^a = \arg \min_{\mathcal{T}} \ell_t^a(\mathcal{T}), \quad (\text{S16})$$

where

$$\begin{aligned} \ell_t^a(\mathcal{T}) = & \mathbb{E} \left[ \|M(b_{o,1}^a, b_{o,2}^a, b_{o,3}^a) \mathcal{T} - M(b_{o,4}^a, b_{o,5}^a, b_{o,6}^a)\|_F^2 \right] + \\ & \lambda_t^a \|\mathcal{T}\|_F^2. \end{aligned} \quad (\text{S17})$$

Similar to the unary case discussed above,

$$\mathcal{T}_t^a = A^{-1}B \quad (\text{S18})$$

where

$$A = \mathbb{E} [M(b_{o,1}^a, b_{o,2}^a, b_{o,3}^a)^T M(b_{o,1}^a, b_{o,2}^a, b_{o,3}^a)] + \lambda_t^a I \quad (\text{S19})$$

and

$$B = \mathbb{E} [M(b_{o,1}^a, b_{o,2}^a, b_{o,3}^a)^T] \mathbb{E} [M(b_{o,4}^a, b_{o,5}^a, b_{o,6}^a)]. \quad (\text{S20})$$

Correspondingly, the answer representation can be obtained by first executing the ternary operator  $\mathbb{E} [M(b_{o,4}^a, b_{o,5}^a, b_{o,6}^a)] \mathcal{T}_t^a$  and slicing it from the result.

To compute the operator distribution, we model it based on the fitness of each operator type,

$$P(\mathcal{T}^a = \mathcal{T}_u^a \mid \{I_{o,i}\}_{i=1}^8) \propto \exp(-\ell_u^a(\mathcal{T}_u^a)) \tag{S21}$$

$$P(\mathcal{T}^a = \mathcal{T}_b^a \mid \{I_{o,i}\}_{i=1}^8) \propto \exp(-\ell_b^a(\mathcal{T}_b^a)) \tag{S22}$$

$$P(\mathcal{T}^a = \mathcal{T}_t^a \mid \{I_{o,i}\}_{i=1}^8) \propto \exp(-\ell_t^a(\mathcal{T}_t^a)). \tag{S23}$$

## B SYSTEMATIC SPLITS AND IN-DISTRIBUTION RESULTS

In the original work of Zhang et al. (2019a) and Hu et al. (2020), there are four operators: Constant, Progression, Arithmetic, and Distribute of Three. Progression is parameterized by its step size ( $\pm 1/2$ ). Arithmetic includes addition and subtraction. And Distribute of Three is implemented as shifting and can be either a left shift or a right one. Note that Constant can be regarded as special Progression with a step size of 0. In this work, we group all four operators into three types: unary (Constant and Progression), binary (Arithmetic), and ternary (Distribute of Three).

To study systematic generalization in abstract relation learning, we use the RPM generation method proposed in Zhang et al. (2019a) and Hu et al. (2020) and carefully split data into three regimes:

- **Systematicity:** The training set and the test set contain all three types of operators but disjoint instances. Specifically, the training set has Constant, Progression of  $\pm 1$ , addition in Arithmetic, and left shift in Distribute of Three, while in the test set there are Progression of  $\pm 2$ , subtraction in Arithmetic, and right shift in Distribute of Three.
- **Productivity:** The training set contains only unary operators and the test set only binary operators. Specifically, the training set has Constant and all instances of Progression, while the test set all instances of Arithmetic.
- **Localism:** The training set contains only binary operators and the test set only unary operators. Specifically, the training set has all instances of Arithmetic and the test set Constant and all instances of Progression.

Please see Figs. S1 to S3 for examples in the three splits.

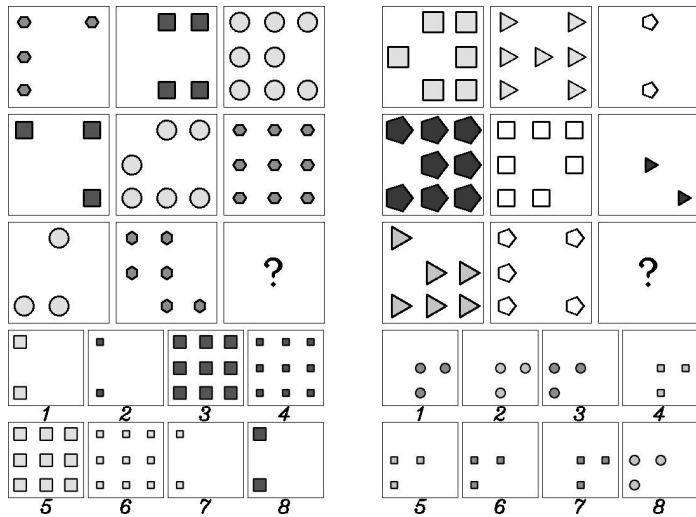


Figure S1: A training example (left) and a test example (right) in the systematicity split. Note that in the training example, the arithmetic relation (in number) is addition and the shifting is always a left shift (in type, size, and color). In the test example, the shifting becomes a right shift (in type), the size progression has a step of 2, and the color arithmetic becomes subtraction.



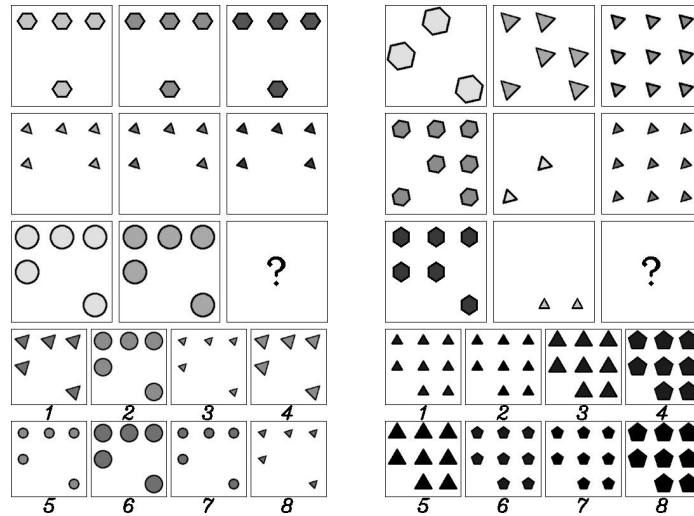


Figure S2: A training example (left) and a test example (right) in the productivity split. Note that in the training example, the constant rule is applied to number, type, and size, while the progression rule is applied on color. In the testing example, the arithmetic rule is applied on all attributes.

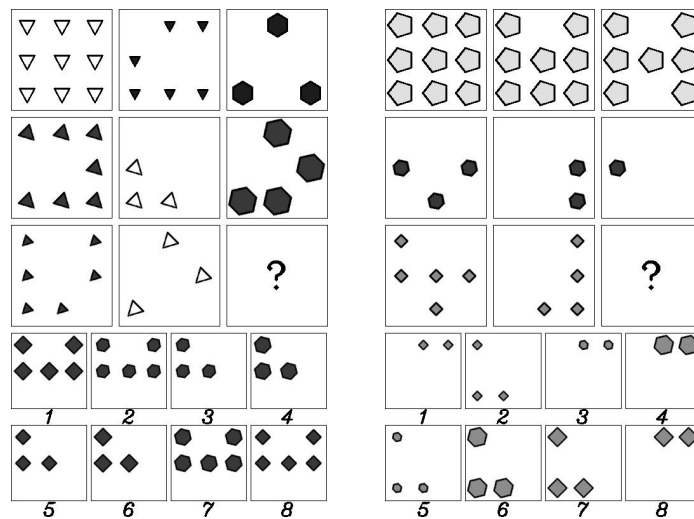


Figure S3: A training example (left) and a test example (right) in the localism split. Note that in the training example, the arithmetic rule is on all attributes. In the test example, the progression rule is applied on number and the constant rule on all other attributes.

Table S1: Model performance on the original datasets for in-distribution evaluation. The performance is measured by accuracy on the test sets. Upper: results on Zhang et al. (2019a). Lower: results on Hu et al. (2020).

Method	Acc	Center	2x2Grid	3x3Grid	L-R	U-D	O-IC	O-IG
ALANS	74.4%	69.1%	80.2%	75.0%	72.2%	73.3%	76.3%	74.9%
HriNet	45.1%	66.1%	40.7%	38.0%	44.9%	43.2%	47.2%	35.8%
CoPINet	91.4%	95.1%	77.5%	78.9%	99.1%	99.7%	98.5%	91.4%
ALANS	78.5%	72.3%	79.5%	72.9%	79.2%	79.6%	85.9%	79.9%
HriNet	60.8%	78.2%	50.1%	42.4%	70.1%	70.3%	68.2%	46.3%
CoPINet	46.1%	54.4%	36.8%	31.9%	51.9%	52.5%	52.2%	42.8%
Human	84.41	95.45	81.82	79.55	86.36	81.81	86.36	81.81

Table S2: The network architecture used for each branch of the object CNN.

Operator	Parameters
Convolution	[6, 5, 1]
BatchNorm	6
SoftPlus	
MaxPool	2
Convolution	[16, 5, 1]
BatchNorm	16
SoftPlus	
MaxPool	2
Linear	120
SoftPlus	
Linear	84
SoftPlus	
Linear	$m$
LogSoftMax	

Table S1 shows the results of the ALANS learner on the original datasets for in-distribution evaluation compared to previous published state-of-the-art. Notably, the ALANS learner is relatively consistent across the two datasets, though inferior on Zhang et al. (2021) potentially due to shortcuts in it that can be better leveraged by neural models.

## C IMPLEMENTATION DETAILS

### C.1 NETWORK ARCHITECTURE

We use a LeNet-like architecture (LeCun et al., 1998) for each branch of the object CNN. See Table S2 for the design. Note that the object CNN consists of four branches, including objectiveness, type, size, and color. The parameters for Convolution denote the output channel size, kernel size, and stride, respectively. A BatchNorm layer is parameterized by the number of channels, whereas a MaxPool layer by its stride. An output size is used to specify parameters of a Linear layer.  $m$  equals 2, 5, 6, 10 for objectiveness, type, size, and color, respectively. For numerical stability, we use LogSoftMax to turn a probability simplex into its log space.

### C.2 OTHER HYPERPARAMETERS

For the inner regularized linear regression, we set different regularization coefficients for different attributes but, for the same attribute, we keep them the same across all three types of operators. For position,  $\lambda = 10^{-4}$ . For number,  $\lambda = 10^{-6}$ . For type,  $\lambda = 10^{-6}$ . For size,  $\lambda = 10^{-6}$ . For color,  $\lambda = 5 \times 10^{-7}$ . All of the regularization terms in Eq. (10) in the main text are set to be 1 and  $\{M_0^a\}$  and  $\{M^a\}$  are initialized as  $2 \times 2$  square matrices.

For training, we first train for 10 epochs parameters regarding objectiveness, including the objectiveness branch, and the representation matrices on position and number. We then perform 2 rounds of cyclic training on parameters regarding type, size, and color, each of which experiences 10 epochs of updates in a round. Finally, we fine-tune all parameters for another 10 epochs, totaling up to 80 training epochs. The entire system is optimized using ADAM (Kingma & Ba, 2014) with a learning rate of  $9.5 \times 10^{-5}$ .

## D MARGINALIZATION FOR OTHER ATTRIBUTES

For the attribute of position, we denote its value as  $R^o$ , a binary vector of length  $N$ , with each entry corresponding to one of the  $N$  windows. Then

$$P(\text{Position} = R^o) = \prod_{j=1}^N P(r_j^o = R_j^o), \quad (\text{S24})$$

where  $P(r_j^o)$  denotes the  $j$ th region’s estimated objectiveness distribution returned by a CNN as in the main text.

For the attribute of type, the panel attribute of type being  $k$  is evaluated as

$$P(\text{Type} = k) = \sum_{R^o} \left( \prod_{j, R_j^o=1} P(r_j^t = k) \right) P(\text{Position} = R^o), \quad (\text{S25})$$

where  $P(r_j^t)$  denotes the  $j$ th region’s estimated type distribution returned by a CNN.

The computation for size and color is exactly the same as type, except that we use the region’s estimated size and color distribution returned by a CNN.

## E MORE ON NEURAL VISUAL PERCEPTION

- **Why not train a CNN to predict the position and number of objects?** The CNN is trained to predict the type, size, color, and object existence in a window. The object existence in windows is marginalized to be a Number distribution and Position distribution. This is a light-weight method for object detection. Nevertheless, it is also possible to use a Fast-RCNN like method to predict object positions (this implies number) directly. However, in this way, the framework loses the probabilistic interpretation (the object proposal branch is currently still deterministic), and we cannot perform end-to-end learning.
- **How does the CNN predict the presence of an object, its type, size, and color given that it is not trained to do that?** For each window, the CNN outputs 4 softmaxed vectors, corresponding to the probability distributions of object existence, object type, object size, and object color. The spaces for these attributes are pre-defined. CNN’s weights are then jointly trained in the framework. Such a design follows recent neuro-symbolic methods (Han et al., 2019; Mao et al., 2019) that also rely on the implicitly trained representation. In short, we assign semantics to the implicitly trained representation (probability distributions for attributes), performs marginalization and reasoning **as if** they are ground-truth attribute distributions, and jointly train using only the problem’s target label.

## F MORE ON ALGEBRAIC ABSTRACT REASONING

- **Are the learned operators interpretable and aligned with ground-truth?** As different operators are of different shapes and are represented as matrices with multiple entries, it’s hard to quantitatively evaluate the fitness in general. However, we have noticed the following patterns of the learned matrices in our case-by-case examination: (1) Approximate permutation matrices for the shifting operation in unary operators (Progression in position) and ternary operators (Distribute of Three). Algebraically, shifting elements in a vector is exactly implemented as the product with a permutation matrix in the representation theory. (2) Approximate identity matrix that keeps the distribution the same and it corresponds

to the Constant relation. (3) Approximate successor matrices that can be understood as Progression when multiplied.